Program Digest, 2019 IEEE International Ultrasonics Symposium (IUS)
Glasgow, Scotland, October 6-9, 2019

Submillimeter Magnetic Microrobot Tracking Using an Integrated Ultrasound and Photoacoustic Imaging System

Yan Yan
Biomedical Engineering
Wayne State University
Detroit, MI, USA
yyan2@wayne.edu

Wuming Jing
A. Linton Department of Mechanical Engineering
Lawrence Technological University
Southfield, MI, USA
wjing@ltu.edu

Mohammad Mehrmohammadi
Biomedical Engineering
Wayne State University
Detroit, MI, USA
mehr@wayne.edu

***Abstract*— This paper presents the proof-of-concept study on a non-invasive tracking of submillimeter sized micro-robotic objects by using combined ultrasound and photoacoustic imaging. Tracking one single microscale untethered magnetic microrobot through the integrated ultrasound and photoacoustic (USPA) imaging will allow for accurate real-time controlling the manipulation of the microrobot in optically non-transparent biological tissues. In this work, the magnetic microrobot prototypes are made from photoresist mixed with nickel particles. Single microrobot agent is set in a fluid environment bounded by an opaque phantom. The experimental results prove that the current microrobot prototypes smaller than 100 μm can be detected by USPA imaging through 15 mm thick opaque phantom, both statically and in a motion of speed approximately 1.5 mm/s. The further investigation of this concept will advance the integration of both non-invasive magnetic manipulation and USPA tracking of the microrobot, targeting the real biomedical applications in the tiny enclosed workspaces.**

Keywords—Photoacoustic, Ultrasound, Imaging, Submillimeter Microrobot.

I. Introduction

Micro-scale untethered mobile robots have been envisioned as one of the next generation intelligent robotic systems [1]. The extremely small size of the mobile microrobots allows for non-invasive operation in the tiny enclosed workspace, such as the potential non-invasive biomedical applications in the circulatory, urinary, and central nervous systems, etc. [2, 3]. One major difficulty in biomedical diagnosis and treatment is the invisibility and inaccessibility under in-vivo condition [4]. The unavoidable invasive practices will usually cause considerable side effects including painful recovery process and certain failure risk [5]. In contrast, the micro-scale microrobots have shown potential to perform as tiny "surgeon" or delivery "vehicle" to achieve non-invasive inner body diagnostic, surgical and therapeutic purposes, that currently only can be realized through conventional invasive biomedical practice.

Among the explored working principles for micro-scale microrobots, magnetic actuation has demonstrated attractive merits and promising results because of its wireless actuation in the non-engineered working environment. The submillimeter scale magnetic microrobot has been demonstrated driven directly by the external magnetic field gradient. To indicate the microrobots moved accordingly, most of the current magnetic microrobot prototypes are working based on the optical vision and tracking system. Optical imaging possesses high definition on the micro-scale, but it requires an open path to the targeting zone. This will cancel the microrobot's substantial merit of non-invasion to the nontransparent biological tissue. The critical non-invasive merit of microrobotic operation cannot be fulfilled without precise feedback in a non-invasive manner. The non-invasive high precision localization and real-time tracking are critical for the microrobot to function properly. Other imaging modality, ultrasound (US) imaging, had been discovered as a non-invasive tracking tool for microrobots [6, 7], which is a widely used safe clinical imaging modality in major clinical operations [8]. However, clinical US imaging has a significant tradeoff between its spatial resolution and penetration depth [9]. In other words, tracking smaller objects will require higher frequency which limits the imaging penetration depth. A typical clinical US system operating at 5 MHz frequency and with a fractional bandwidth of 80% will have an axial resolution of around 200 μm. In addition, the ability of US imaging in tracking small-scale objects such as microrobots is highly affected by the contrast and contrast-to-noise ratio (CNR) due to similarity in echogenicity of the objects and surrounding background tissue. The tracking of magnetic microrobots in [6] and [7] is either based on bubbles emitted from the microjet or based on a large swarm of agents, which are both on the mm scale. The low sensitivity of clinical US images confines its application int he area of advanced biomedical imaging. In contrast, photoacoustic (PA) imaging is a burgeoning US integrated imaging modality that has shown tremendous potential in diagnostic applications by providing complementary functional and molecular information [10-16]. PA imaging utilizes a nanosecond short laser pulse to the targeted object whose molecules absorb the light energy and cause rapid thermal expansion and thus generating acoustic waves. With a US probe, the resulted acoustic signal from micro-meter, even nano-meter sized object can be detected and evaluated. This integrated USPA method is more sensitive than ultrasound alone and can provide more functional and molecular information.

Therefore, the work presented in this paper is our initial effort to incorporate integrated USPA imaging in order to track

single micro-scale microrobot in the non-transparent environment, which will allow for the whole microrobot system working in a non-invasive manner in the future. The following section II introduces the magnetic microrobot prototypes and the experimental setup of photoacoustic imaging. The experimental results of the imaging tests will be demonstrated and analyzed in section III. In the conclusion section IV, further integration of the microrobot and photoacoustic imaging will be discussed in order for potential real biomedical operation trials.

II. Materials and Methods

A. Magnetic Microrobot

Series of different sizes magnetic microrobots are prepared for the imaging tests using integrated ultrasound and photoacoustic (USPA) principle. In order to enhance the absorption of photon signals for better imaging result, the nickel (Ni) microparticles (Alfa Aesar) is adopted to fabricate the magnetic microrobot prototypes. The average diameter of the particles is approximately 3-7 µm that fits in the microrobot's envelope dimension well. The 99.9% metals basis particle and also its dark grey to black color will induce strong absorption of photonic signals, which generates strong imaging contrast. The Ni particles are mixed in the negative photoresist SU-8 2035 (MicroChem) in a density of 1:25 g/mL (Volume ratio ≈ 1:7). The sample is then patterned through photolithography to produce the microrobot prototypes in varied dimensions (400 µm, 200 µm, 100 µm, 50 µm square, **Fig. 1**). The thickness of the developed microrobots is approximately 40 µm. The varied sizes of single microrobot agent will not only gauge the imaging capacity of the USPA, and also compare out the pure US imaging and USPA imaging.

B. Integrated Ultrasound and Photoacoustic (USPA) Imaging

The integrated USPA is an advanced biomedical imaging method combining the advantages from both US and PA. It provides co-registered bio-tissue background morphology (US) with high contrast images of the microrobots (PA) at relatively high penetration depth [17]. The US imaging can demonstrate tissue background with high detail for biological analysis. PA imaging, on the other hand, can highlight the light absorbers (i.e. microrobots in this case) in the illuminated regions with better sensitivity and contrast on micro-scale objects. Therefore, the integrative USPA images will be an ideal solution to track micro-scale microrobot in the enclosed working environment. It can simultaneously provide structural information of the enclosed environment, and also perform functional tracking through highlighted microrobot agent. The frame rate of USPA modality will also facilitate the tracking of the microrobot in real-time.

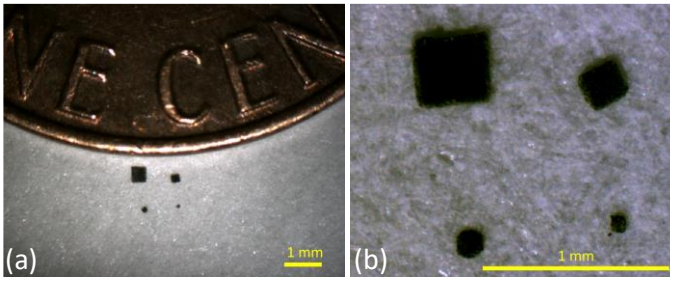

Figure 1. Magnetic microrobot prototypes of different sizes (400 µm, 200 µm, 100 µm, 50 µm) under optical camera. (a) Microrobot prototypes compared to a US penny coin. (b) 5*X* zoomed in view from (a) for the microrobots.

The imaging system (**Fig. 2**) consists of a tunable optical parametric oscillator (OPO) pumped with a high energy short-pulsed laser (OPOTEK core, 650 nm to 2400 nm, 10 Hz, 8 ns pulse duration). The beam from the laser was coupled to a fiber bundle with 19 fibers (Thorlabs, multimode, 1000 µm core size, silica/TECS clad, NA=0.39). A clinical linear array US transducer (L11-4v, 4-11 MHz bandwidth), connected to a US research platform (Verasonics, Vantage 128) were used to acquire the co-register US and PA images.

III. Results and Discussion

A. USPA Imaging of Static Microrobot

In order to verify the sensitivity and resolution of USPA imaging on the microrobots. Multiple microrobot prototypes with four different sizes are manually placed into an "L•••W" pattern, the two initial letters of collaborating universities (**Fig. 3a**). To ensure the static stance of microrobots, the workspace is filled with a liquid medium of high viscosity (Purell, 3659-12). After the workspace is enclosed, the PA images were acquired at laser wavelength (λ) set to =680 nm. The choice of 680 nm wavelength for PA imaging is to demonstrate the utility of PA in tracking microrobots at a wavelength that is suitable for future clinical applications, where the depth of penetration is required for tracking objects. Since the designed magnetic microrobot is made with nickel particle, which is strong optical absorber across all visible wavelength and the fluence of the laser illumination is set within the clinical safety requirements (< 25 mJ/cm^2). As shown in **Figure 3b**, the PA imaging is capable of detecting the microrobots from size 400 µm down to approximately 50 µm (with a 25% threshold level in the cumulative distribution). It is also noted that the largest microrobot prototypes are showing the highest amplitude of PA signals.

For comparison purpose, the same set of microrobot prototypes was also imaged through pure US method (**Fig. 3c**).

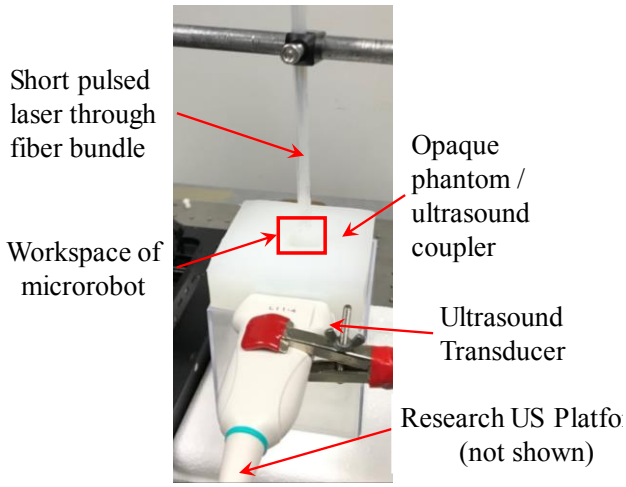

Figure 2. Integrated ultrasound and photoacoustic (USPA) imaging setup for tracking microrobot.

It is known that the axial resolution of the US depends on the transmitted center frequency. During the experiment the transmit center frequency was set to 11 MHz, which corresponds to an axial resolution of 120 µm. From the detected images we can indicate the smaller (50 and 100 µm) microrobot prototypes are completely invisible under US imaging mode. The 200 µm microrobots are barely detected. The 400 µm ones constituted "L" shape is detected. Compared to the "L" in PA imaging result, the blurs between microrobots on the US image indicate the existence of reverberation, since the microrobots closer to the US transducer probe will block part of the acoustic wave reflected from the farther ones. We compared the CNR in the US and PA images. In the PA image, the 50, 100, and 200 µm size microrobots had an average CNR of 25.3 dB, and 400 µm size microrobots had a CNR of 47.4 dB. In US images, the 50, 100, and 200 µm size microrobots had nearly 0 dB CNR, and 400 µm size microrobots had a CNR of 7.1 dB.

B. USPA Imaging for Microrobot in Motion

As a proof-of-concept for non-invasive tracking of single micro-scale mobile microrobot, the USPA imaging test is also performed when the magnetic microrobot is in motion. In this study, two sizes (400 µm and 100 µm) microrobots are selected to evaluate the sensitivity of USPA imaging to track the moving microrobots. During the experiments, only one single microrobot was placed in workspace successively. Distal (DI) water is filled in the workspace as motion medium and for acoustic coupling. The imaging time resolution of PA and US are 10 Hz and 30 Hz, respectively.

The microrobot is actuated by a static magnetic field. The acting magnetic force F_m is evaluated as:

$$F_m = \nabla(\mathrm{m} \cdot \mathrm{B}) = m \cdot \nabla B \qquad (1)$$

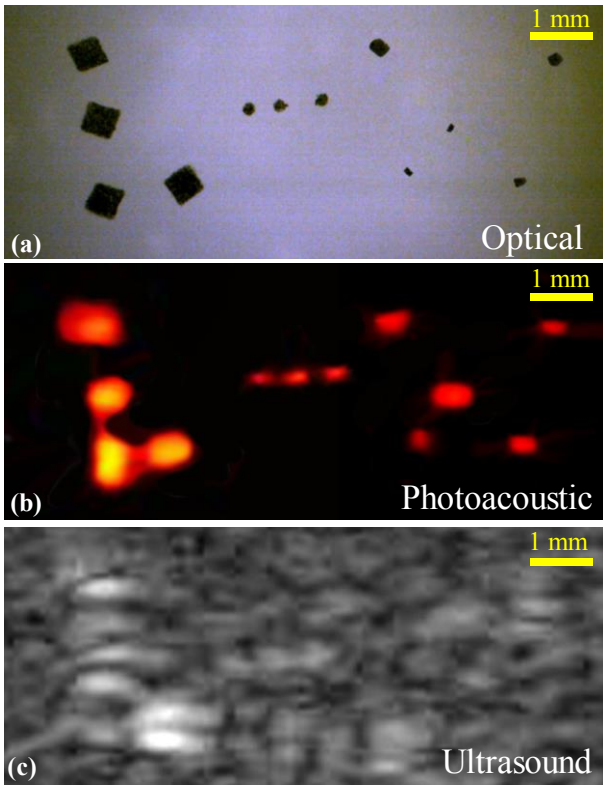

Figure 3. Imaging result of inactive microrobots with different sizes in a pattern of "L•••W". (a) Reference photo through the optical camera in open workspace. (b) The photoacoustic image in the enclosed workspace. (c) Ultrasound image.

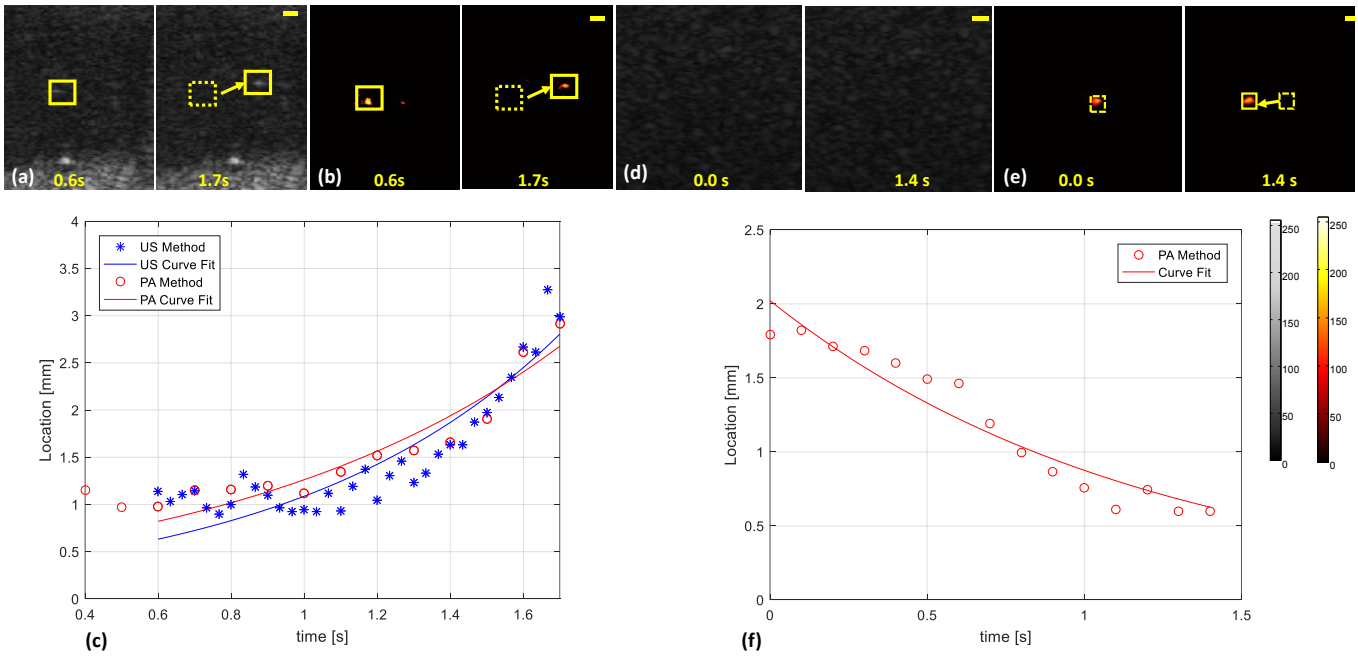

Figure 4. USPA imaging results for microrobots in motion. (a, b) The start and end frame of the 400 µm microrobot in motion. (c) Detected motion track of the 400 µm microrobot in a static magnetic field. (d, e) The start and end frame of the 100 µm microrobot. (f) Detected motion track of the 100 µm microrobot in a static magnetic field. The scale bars are 1 mm.

where *m* is the magnetization of the nickel material that is treated as a constant value. Therefore, ∇B along the acting direction is the governing factor to determine acting magnetic force. As shown in **Figure 4a** and **4b**, this approximately 2 mm motion of a 400 µm microrobot is tracked by both US and PA imaging methods. The detailed tracking results are plotted in **Figure 4c**. Assume the microrobot moves in uniform acceleration a starting from stationary status. Then it can be assessed through

$$a = \frac{2S}{t^2} \quad (2)$$

where S is the traveled distance and t is the elapsed time. The microrobot had an acceleration of 3.3 mm/s^2. According to Newton's second law, the driving force needed is approximately $2.6\times 10^{-11}N$, which is a result of magnetic during force as well as other acting forces such as fluid tension and electrostatic forces. For imaging, we also noted that the 10 Hz PA imaging and 30 Hz US imaging is showing approximately 5% difference on-location estimation. Considering the better sensitivity of PA imaging, it may be mainly due to the non-accurate visualization of US imaging.

In order to further compare the sensitivity of PA and US imaging for the microrobots in motion, the same experiment is performed on a smaller microrobot prototype (100 µm), which is beyond the resolution of the US method. The imaging settings of US and PA methods are also kept the same as the previous test. As shown in **Figure 4d** and **4e**, the US imaging cannot detect this single microrobot prototype but only background signals. In contrast, PA imaging method still can track the microrobot with strong signal amplitude. Based on the tracked motion fact (**Fig. 4f**), the acceleration is measured as 2.1 mm/s^2.

IV. Conclusions and Future Work

This paper reports the preliminary work for non-invasive tracking of a single micro-scale magnetic microrobot using the integrated ultrasound and photoacoustic (USPA) imaging. The USPA imaging can successfully visualize the microrobot prototype as small as 50 µm. The experimental results verify that USPA imaging modality is more sensitive than pure US imaging. The PA imaging shows better sensitivity on the dimension. The USPA imaging test of the microrobot in motion also provides proof-of-concept for the integrative working mode of USPA imaging and magnetic manipulation of the microrobot. These two both non-invasive modalities will allow for potential complete non-invasive operation of intelligent micro-scale microrobots for in vivo biomedical applications. Further future works will focus on the integration of the magnetic manipulation system and the USPA imaging system. The better understanding of the interaction between magnetic manipulation and USPA imaging will advance future autonomous closed-loop control of non-invasive micro-robotic tools.

References

[1] S. Palagi and P. Fischer, "Bioinspired microrobots," *Nature Reviews Materials,* p. 1, 2018.

[2] C. Chautems, B. Zeydan, S. Charreyron, G. Chatzipirpiridis, S. Pane, and B. J. Nelson, "Magnetically powered microrobots: a medical revolution underway?," *European Journal of Cardio-Thoracic Surgery,* vol. 51, no. 3, pp. 405-407, 2017.

[3] M. Sitti *et al.*, "Biomedical applications of untethered mobile milli/microrobots," *Proceedings of the IEEE,* vol. 103, no. 2, pp. 205-224, 2015.

[4] A. L. Goldstein and D. Soffer, "Trauma to the heart: A review of presentation, diagnosis, and treatment," *Journal of Trauma and Acute Care Surgery,* vol. 83, no. 5, pp. 911-916, 2017.

[5] T. L. Demmy, S. Yendamuri, T. A. D'Amico, and W. R. Burfeind, "Oncologic equivalence of minimally invasive lobectomy: the scientific and practical arguments," *The Annals of thoracic surgery,* vol. 106, no. 2, pp. 609-617, 2018.

[6] A. Sánchez, V. Magdanz, O. G. Schmidt, and S. Misra, "Magnetic control of self-propelled microjets under ultrasound image guidance," in *5th IEEE RAS/EMBS International Conference on Biomedical Robotics and Biomechatronics*, 2014, pp. 169-174: IEEE.

[7] Q. Wang, L. Yang, J. Yu, C.-I. Vong, P. W. Y. Chiu, and L. Zhang, "Magnetic Navigation of a Rotating Colloidal Swarm Using Ultrasound Images," in *2018 IEEE/RSJ International Conference on Intelligent Robots and Systems (IROS)*, 2018, pp. 5380-5385: IEEE.

[8] T. L. Szabo, *Diagnostic ultrasound imaging: inside out*. Academic Press, 2004.

[9] S. K. Edelman, *Understanding ultrasound physics*. Baker & Taylor, 2003.

[10] M. Mehrmohammadi, S. Joon Yoon, D. Yeager, and S. Y Emelianov, "Photoacoustic imaging for cancer detection and staging," *Current molecular imaging,* vol. 2, no. 1, pp. 89-105, 2013.

[11] M. Basij *et al.*, "Miniaturized phased-array ultrasound and photoacoustic endoscopic imaging system," *Photoacoustics,* vol. 15, p. 100139, 2019.

[12] Y. Yan, S. John, M. Ghalehnovi, L. Kabbani, N. A. Kennedy, and M. Mehrmohammadi, "photoacoustic Imaging for Image-guided endovenous Laser Ablation procedures," *Scientific reports,* vol. 9, no. 1, p. 2933, 2019.

[13] Y. Yan *et al.*, "Photoacoustic imaging of the uterine cervix to assess collagen and water content changes in murine pregnancy," *Biomedical Optics Express,* vol. 10, no. 9, pp. 4643-4655, 2019.

[14] S. S. Alshahrani *et al.*, "All-reflective ring illumination system for photoacoustic tomography," *Journal of biomedical optics,* vol. 24, no. 4, p. 046004, 2019.

[15] N. Alijabbari, S. S. Alshahrani, A. Pattyn, and M. Mehrmohammadi, "Photoacoustic Tomography with a Ring Ultrasound Transducer: A Comparison of Different Illumination Strategies," *Applied Sciences,* vol. 9, no. 15, p. 3094, 2019.

[16] L. V. Wang and S. Hu, "Photoacoustic tomography: in vivo imaging from organelles to organs," *science,* vol. 335, no. 6075, pp. 1458-1462, 2012.

[17] M. H. Xu and L. H. V. Wang, "Photoacoustic imaging in biomedicine," (in English), *Review of Scientific Instruments,* vol. 77, no. 4, Apr 2006.